ELectronics EXpress

LETTER

IEICE Electronics Express, Vol.12, No.17, 1–8

Simple quasi-static analysis for coplanar stripline within multilayer dielectrics

Jaeyul Choo[1], Chihyun Cho[2], and Jaegul Choo[3a)]

[1] *Department of Instrumentation, Control and Electrical System, Korea Institute of Nuclear Safety, 62 Gwahak-ro, Yuseong-gu, Daejeon 305–338, Korea*

[2] *Center for Electromagnetic Wave, Korea Research Institute of Standards and Science, 267 Gajeong-ro, Yuseong-gu, Daejeon 305–340, Korea*

[3] *Department of Computer Science and Engineering, Korea University, Anam-dong 5-ga, Seongbuk-gu, Seoul 136–713, Korea*

a) *jchoo@korea.ac.kr*

Abstract: We apply the mode-matching method to the analysis of coplanar striplines surrounded by multilayer dielectrics and lateral conductive shields. Then the characteristic impedances and the effective dielectric constants of various coplanar striplines are calculated based on assumption that the electromagnetic coupling between the lateral shield and striplines could be neglected with a proper condition. Also we verify the accuracy of the mode-matching method compared with the conformal mapping technique.

Keywords: mode-matching method, effective dielectric constant, characteristic impedance

Classification: Electromagnetic theory

References

[1] K. C. Gupta, R. Garg, I. Bahl and P. Bhartia: *Microstrip Lines and Slotlines* (Artech House, MA, 1996) 2nd ed. ch. 2.

[2] S. X. Ta and I. Park: J. Electromagn. Eng. Sci. **13** (2013) 22. DOI:10.5515/JKIEES.2013.13.1.22

[3] N. Morita, K. Ohno and H. Fukushima: IEICE Trans. Electron. **E86-C** (2003) 1480.

[4] M. Tsuji and H. Shigesawa: IEICE Trans. Electron. **E83-C** (2000) 720.

[5] I. F. Chen and C. W. Hsue: IEICE Trans. Commun. **E85-B** (2002) 2924.

[6] N. G. Alexópoulos: IEEE Trans. Microw. Theory Techn. **MTT-33** (1985) 847. DOI:10.1109/TMTT.1985.1133145

[7] C. Yildiz, K. Guney, M. Turkmen and S. Kaya: PIER **69** (2007) 127. DOI:10.2528/PIER06120802

[8] D. Packiaraj, K. J. Vinoy, M. Ramesh and A. T. Kalghatgi: J. Electromagn. Waves Appl. **27** (2013) 856. DOI:10.1080/09205071.2013.789410

[9] G. Chione and C. Naldi: Electron. Lett. **20** (1984) 179. DOI:10.1049/el:19840120

[10] E. Chen and S. Y. Chou: IEEE Trans. Microw. Theory Techn. **45** (1997) 939. DOI:10.1109/22.588606

[11] C. M. Kim and R. V. Ramaswamy: J. Lightwave Technol. **7** (1989) 1063. DOI:10.1109/50.29633

© IEICE 2015

DOI: 10.1587/elex.12.20150361
Received April 17, 2015
Accepted May 11, 2015
Publicized June 11, 2015
Copyedited September 10, 2015

[12] D. Kim, H. J. Eom and Y. S. Lee: IEICE Electron. Express **11** (2014) 20140219. DOI:10.1587/elex.11.20140219
[13] J. Choo, H. J. Eom and D. Kim: IEEE Antennas Wireless Propag. Lett. **12** (2013) 445. DOI:10.1109/LAWP.2013.2254461
[14] H. J. Eom: *Wave Scattering Theory* (Springer Verlag, Berlin, 2001).
[15] H. J. Eom: *Electromagnetic Wave Theory for Boundary-value Problems* (Springer Verlag, Berlin, 2004).

1 Introduction

Coplanar stripline (CPS) is one of the most popular transmission lines in microwave-integrated circuits (MICs) due to its good propagation characteristics, such as small dispersion and lower losses [1, 2]. Lots of approaches have been previously introduced to analyze various properties of CPS [1, 3, 4, 5, 6, 7, 8].

The conformal mapping technique is often used for the interpretation of the CPS due to its simple closed-form expression [9, 10, 11]. However, an asymmetric stripline placed on the multilayer substrate requires the superposition principle in the conformal mapping technique, and it would lead to complicated formulation [10]. Another widely-used approach is the mode-matching method, which has been utilized in the analyses of many types of planar striplines [12, 13, 14, 15]. In addition, the quasi-static analysis allows the mode-matching method to be applied to the calculation of the multiple striplines [9, 13].

In this paper, a general quasi-static solution for the asymmetric CPS surrounded with multilayer dielectrics is derived using the mode-matching method. For the quasi-static boundary condition, we introduce lateral conductive shields to the CPS structure. Then, the proper distance to prevent electromagnetic coupling between the lateral shields and stripline is derived from the field distribution and the capacitance matrix. Finally, the effective dielectric constant and the characteristic impedance are calculated based on the distance analysis. Note that the novelty of this research is the consideration of asymmetric CPS within multilayer dielectrics. In what follows, we show a brief mode-matching formulation on the potential distribution and boundary conditions for simultaneous equations.

2 Mode-matching formulation

Fig. 1 illustrates a cross section of the CPS surrounded by multilayer dielectrics with lateral conducting shields of 0 V. The potentials V_1 and V_2 are applied to two striplines with the width w_1 and w_2, respectively, and the separating distance s. The surrounding dielectrics are specifically divided into three different regions, which are regions u_k with ε_{uk} $(k = 1, 2, 3, \cdots)$ for the upper dielectrics, regions b_t with ε_{bt} $(t = 1, 2, 3, \cdots)$ for the bottom dielectrics, and regions 1–3 with ε_1, ε_2, and ε_3 for the dielectrics adjacent to two striplines. The conductive lateral shields stand apart from the CPS with distance d_1 and d_2. From the superposition principle and Laplace's equation, the potential in every region is expressed [14, 15] as

© IEICE 2015
DOI: 10.1587/elex.12.20150361
Received April 17, 2015
Accepted May 11, 2015
Publicized June 11, 2015
Copyedited September 10, 2015

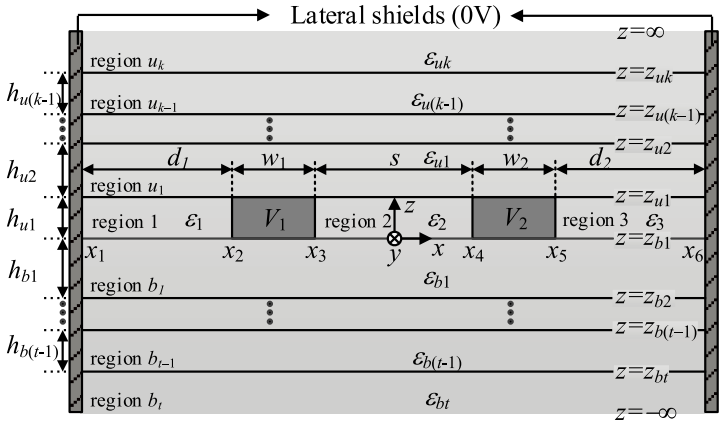

Fig. 1. Cross section of CPS in the multilayer dielectrics.

$$\Phi_1 = \sum_{n_1=1}^{\infty} \sin(m_1(x-x_1)) f_1(z) + \frac{V_1}{d_1}(x-x_1) \quad \text{(in region 1)}, \tag{1}$$

$$\Phi_2 = \sum_{n_2=1}^{\infty} \sin(m_2(x-x_3)) f_2(z) + \frac{V_2-V_1}{s}(x-x_3) + V_1 \quad \text{(in region 2)}, \tag{2}$$

$$\Phi_3 = \sum_{n_3=1}^{\infty} \sin(m_3(x-x_5)) f_3(z) - \frac{V_2}{d_2}(x-x_6) \quad \text{(in region 3)}, \tag{3}$$

$$\Phi_{uk,bt} = \sum_{n_{uk},n_{bt}=1}^{\infty} \sin(m_{uk,bt}(x-x_1)) f_{uk,bt}(z) \quad \text{(in other regions)}, \tag{4}$$

where $m_1 = n_1\pi/d_1$, $m_2 = n_2\pi/s$, $m_3 = n_3\pi/d_2$, $m_{uk} = n_{uk}\pi/(x_6-x_1)$, $m_{bt} = n_{bt}\pi/(x_6-x_1)$ $(k=t=1,2,3,\cdots)$, and

$$f_\alpha(z) = \begin{cases} A_\alpha e^{-m_\alpha z}, & \text{when } \alpha = uk_{max} \text{ and } k_{max} = \text{maximum } k \\ B_\alpha e^{m_\alpha z}, & \text{when } \alpha = bt_{max} \text{ and } t_{max} = \text{maximum } t \\ A_\alpha e^{-m_\alpha z} + B_\alpha e^{m_\alpha z}, & \text{otherwise} \end{cases}. \tag{5}$$

To determine the unknown modal coefficients A_α and B_α in Eq. (5), the Dirichlet conditions for the continuity of potentials at $z = z_{u1}$ and $z = z_{uk}$ yield Eqs. (6) and (7), respectively. The Neumann conditions for the continuity of normal derivatives of the potentials at $z = z_{u1}$ and $z = z_{uk}$ yield Eqs. (8)–(11).

$$\begin{aligned} &\frac{x_1-x_6}{2}\sum_{n_{u1}=1}^{\infty} f_{u1}(z_{u1})\delta_{m_{u1}p_{u1}} + \sum_{n_1=1}^{\infty}[F(x_1,x_2,m_1,p_{u1})f_1(z_{u1})] \\ &\quad + \sum_{n_2=1}^{\infty}[F(x_3,x_4,m_2,p_{u1})f_2(z_{u1})] + \sum_{n_3=1}^{\infty}[F(x_5,x_6,m_3,p_{u1})f_3(z_{u1})] \\ &= -\frac{V_1}{d_1}g(x_1,x_2) + \frac{V_1-V_2}{b}g(x_3,x_4) - \frac{V_2}{d_2}g(x_6,x_5) \\ &\quad + \frac{V_1-V_2}{p_{u1}}\cos p_{u1}(x_1-x_4) - \frac{V_1}{p_{u1}}\cos p_{u1}(x_1-x_2) + \frac{V_2}{p_{u1}}\cos p_{u1}(x_1-x_5) \end{aligned} \tag{6}$$

$$\sum_{n_{u(k-1)}=1}^{\infty} F(x_1,x_6,m_{u(k-1)},p_{uk})f_{u(k-1)}(z_{uk}) + \frac{x_1-x_6}{2}\sum_{n_{uk}=1}^{\infty} f_{uk}(z_{uk})\delta_{m_{uk}p_{uk}} = 0 \tag{7}$$

where

© IEICE 2015
DOI: 10.1587/elex.12.20150361
Received April 17, 2015
Accepted May 11, 2015
Publicized June 11, 2015
Copyedited September 10, 2015

$$F(a,b,m_\alpha,p_\beta)=\int_a^b \sin m_\alpha(x-a)\sin p_\beta(x-x_1)dx,$$

$$g(\beta,\gamma)=\int_\beta^\gamma (x-\beta)\sin p_{u_1}(x-x_1)dx,$$

$p_{uk}=q_{uk}\pi/(x_6-x_1)$, $q_{uk}=1,2,\cdots$, maximum n_{uk}, and δ_{mp} is the Kronecker delta.

$$\frac{\varepsilon_{u1}}{\varepsilon_1}\sum_{n_{u1}=1}^{\infty}F(x_1,x_2,p_1,m_{u1})\frac{df_{u1}(z)}{dz}\bigg|_{z=z_{u1}}+\frac{x_1-x_2}{2}\sum_{n_1=1}^{\infty}\frac{df_1(z)}{dz}\bigg|_{z=z_{u1}}\delta_{n_1p_1}=0 \quad (8)$$

$$\frac{\varepsilon_{u1}}{\varepsilon_2}\sum_{n_{u1}=1}^{\infty}F(x_3,x_4,p_2,m_{u1})\frac{df_{u1}(z)}{dz}\bigg|_{z=z_{u1}}+\frac{x_3-x_4}{2}\sum_{n_2=1}^{\infty}\frac{df_2(z)}{dz}\bigg|_{z=z_{u1}}\delta_{m_2p_2}=0 \quad (9)$$

$$\frac{\varepsilon_{u1}}{\varepsilon_3}\sum_{n_{u1}=1}^{\infty}F(x_5,x_6,p_3,m_{u1})\frac{df_{u1}(z)}{dz}\bigg|_{z=z_{u1}}+\frac{x_5-x_6}{2}\sum_{n_2=1}^{\infty}\frac{df_3(z)}{dz}\bigg|_{z=z_{u1}}\delta_{m_3p_3}=0 \quad (10)$$

$$\frac{\varepsilon_{u(k-1)}}{\varepsilon_{u_k}}\sum_{n_{u(k-1)}=1}^{\infty}F(x_1,x_6,m_{u(k-1)},p_{u_k})\frac{df_{u(k-1)}(z)}{dz}\bigg|_{z=z_{uk}}$$
$$+\frac{x_1-x_6}{2}\sum_{n_{uk}=1}^{\infty}\frac{df_{uk}(z)}{dz}\bigg|_{z=z_{uk}}\delta_{m_{uk}p_{uk}}=0 \quad (11)$$

For the bottom regions, it is possible to enforce the boundary conditions at $z=z_{b1}$ and $z=z_{bt}$ through the similar procedure. The results from the enforcement of boundary conditions constitute a set of simultaneous equations for the modal coefficients A_α and B_α. The modal coefficients are calculated efficiently after truncating the infinite series in the simultaneous equations.

3 Computed results

3.1 Field distribution

The time-invariant electric field $\bar{E}$ is derived from the calculated potential as shown in Eq. (12).

$$\bar{E}=-\nabla\Phi(x,z)=\hat{a}_xE_x+\hat{a}_zE_z=-\left(\hat{a}_x\frac{\partial\Phi(x,z)}{\partial x}+\hat{a}_z\frac{\partial\Phi(x,z)}{\partial z}\right) \quad (12)$$

Fig. 2 shows the electric field distributions of z-component (E_z) and x-component (E_x) for an asymmetric CPS without dielectric layers where geometrical parameters are $w_1=s=10\,\text{mm}$, $w_2=5\,\text{mm}$, $h_{u1}=1\,\text{mm}$, and $d_1=d_2=200\,\text{mm}$. In Fig. 2, the electric fields are normalized by the potential difference between two striplines where the applied potentials are $V_1=-1$ and $V_2=1$. In Fig. 2(a), E_z has high values on the edge of striplines and E_z on the narrow stripline is stronger than that of the wide stripline. In addition, E_x is forceful between lateral shields and striplines and gets strong as the lateral shields approach the striplines in Fig. 2(b). These results indicate that the electromagnetic coupling from the lateral shields depend on the distances d_1 and d_2.

3.2 Electromagnetic coupling from lateral shields

Next, the electromagnetic coupling from lateral shields to striplines is analyzed by the comparison of the capacitance matrix depending on the distance d ($d=d_1=d_2$). Fig. 3 shows the evaluated capacitance matrix as a function of

© IEICE 2015
DOI: 10.1587/elex.12.20150361
Received April 17, 2015
Accepted May 11, 2015
Publicized June 11, 2015
Copyedited September 10, 2015

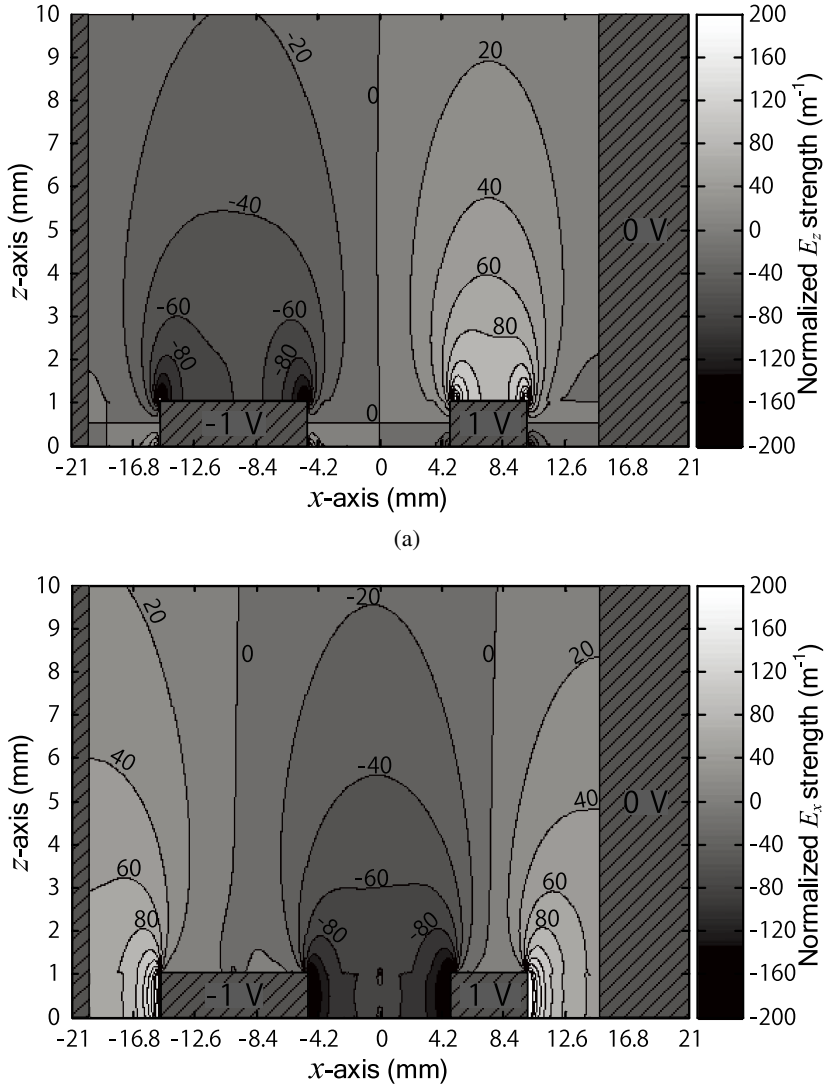

Fig. 2. Electric field distribution of asymmetric CPS without dielectrics with $w_1 = s = 10\,\text{mm}$, $w_2 = 5\,\text{mm}$, $d_1 = d_2 = 200\,\text{mm}$, and $\varepsilon_{b1} = 1$: (a) z-component (E_z) and (b) x-component (E_x).

$d/(2w + s)$. The C_{11} and C_{12} drastically change when the ratio of $d/(2w + s)$ increases from 0 closely to 1. As the ratio approaches about 15 the C_{11} and C_{12} then converge to about 115 and 65, respectively. This investigation would provide proper distance d for avoiding the electromagnetic coupling from the lateral shields. In other words, it is possible that the CPS with the lateral shields is substituted for the one without the lateral shield as the distance d is much larger (over 15 times) than $(2w + s)$. Based on this investigation, we then calculate the effective dielectric constants and the characteristic impedances for various CPSs with enough distance d to neglect the coupling effect from the lateral shields.

3.3 Effective dielectric constants and characteristic impedance

When the potentials on the CPS are $V_1 = -1$ and $V_2 = 1$, the effective dielectric constant (ε_{eff}) and the characteristic impedance (Z_0) are calculated [1], respectively, as

© IEICE 2015
DOI: 10.1587/elex.12.20150361
Received April 17, 2015
Accepted May 11, 2015
Publicized June 11, 2015
Copyedited September 10, 2015

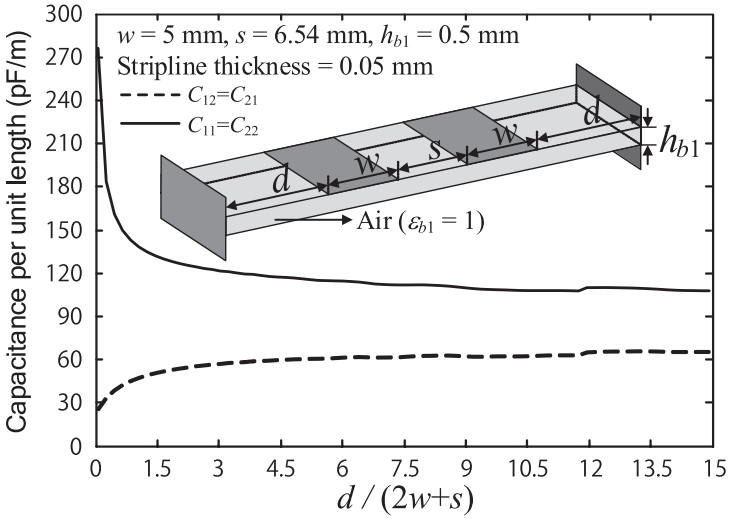

Fig. 3. Capacitance matrix of symmetric CPS on a single layer dielectric with $\varepsilon_{b1} = 1$ when distance d from the lateral shield increases.

$$\varepsilon_{eff} = C/C_{wo} \tag{13}$$

$$Z_0 = 1/c\sqrt{CC_{wo}}, \tag{14}$$

where C is the total line capacitance of CPS, C_{wo} is the total line capacitance without dielectric layers, and c is the speed of light in the free space.

Fig. 4 presents the computed effective dielectric constants and characteristic impedances for a symmetric CPS ($w_1 = w_2 = w$) on a single layer dielectric ($\varepsilon_{b1} = 4.6$ and the thickness of h_{b1}). The results are illustrated as a function of $s/(2w + s)$ for several $h_{b1}/(2w + s)$, and they are compared to the results of the conformal mapping technique [9]. The results show a favorable agreement with the conformal mapping technique. The small discrepancies are attributed to the considered stripline thickness h_{u1} in our approach. The characteristic impedance is

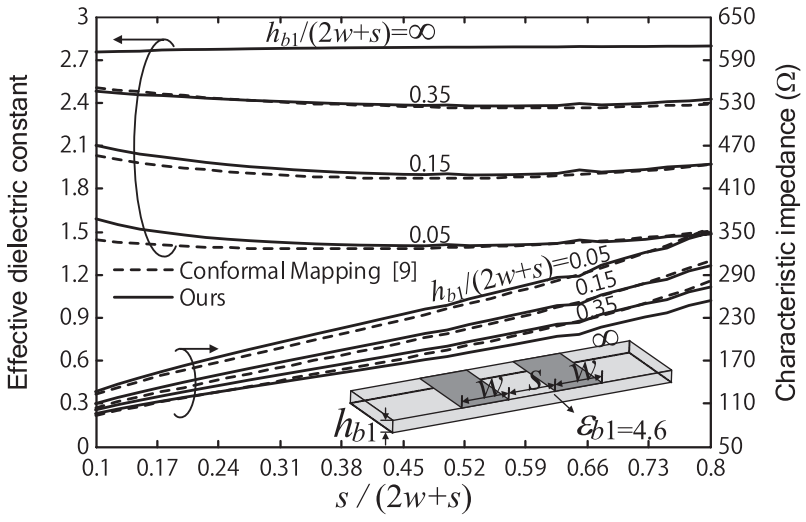

Fig. 4. Effective dielectric constant and characteristic impedance of symmetric CPS on a single layer dielectric with $\varepsilon_{b1} = 4.6$.

© IEICE 2015
DOI: 10.1587/elex.12.20150361
Received April 17, 2015
Accepted May 11, 2015
Publicized June 11, 2015
Copyedited September 10, 2015

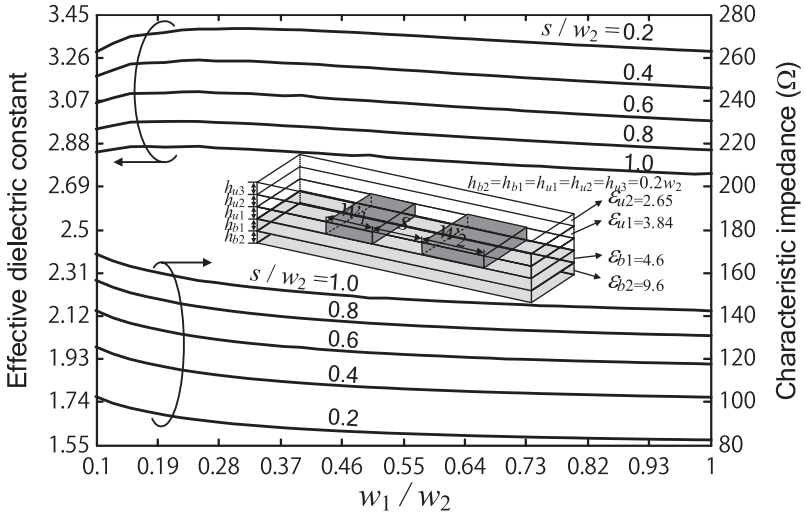

Fig. 5. Effective dielectric constant and characteristic impedance of asymmetric CPS on four layer dielectrics with $h_{b2} = h_{b1} = h_{u1} = h_{u2} = h_{u3} = 0.2w_1$, $\varepsilon_1 = 1$, $\varepsilon_2 = 1$, $\varepsilon_3 = 1$, $\varepsilon_{b2} = 9.6$, $\varepsilon_{b1} = 4.6$, $\varepsilon_{u1} = 3.84$, and $\varepsilon_{u2} = 2.65$.

proportional to $s/(2w + s)$, which decreases as $h_{b1}/(2w + s)$ increases. The effective dielectric constant increases as the $h_{b1}/(2w + s)$ grows whereas the change in $s/(2w + s)$ has little effect on the effective dielectric constant.

Fig. 5 illustrates the computed effective dielectric constants and the characteristic impedances for the asymmetric CPS inserted into multilayer dielectrics. The results are shown as a function of w_1/w_2 for several s/w_2. As the ratio of the distance to the width (s/w_2) grows, the characteristic impedance increases while the effective dielectric constant decreases. As w_1/w_2 increases from 0.1 to 1 (in a symmetric CPS case), the characteristic impedance is shown to gradually decrease while the effective dielectric constant slightly grows and then slowly diminishes, as seen in Fig. 5. Note that there is no limitation for the number of dielectrics enclosing CPSs in our approach.

The dielectric constants and the characteristic impedances for the asymmetric CPS on a single layer dielectric layer are investigated since it is generally employed in MICs. Fig. 6 shows both of these results as functions of w_1/w_2 and s/w_2 when thickness h_{b1} and the permittivity of the single layer are $0.5w_1$ and 4.6 respectively. In this case, the characteristic impedance of the asymmetric CPS (see Fig. 6(a)) is more sensitive to the changes of other parameters when the CPS maintains small w_1/w_2 and large s/w_2. It means that the reproducibility of the characteristic impedance in the manufacturing process is greatly improved as the distance s is reduced and the width of lines is similar to each other. However, the effective dielectric constant (see Fig. 6(b)) shows nearly constant in the range from 2 to 2.3, and it has the smallest value in the condition of around $s/w_2 = 0.1$. The analysis performed in Figs. 4, 5, and 6 would offer the geometrical information of CPS required to design various microwave components.

© IEICE 2015
DOI: 10.1587/elex.12.20150361
Received April 17, 2015
Accepted May 11, 2015
Publicized June 11, 2015
Copyedited September 10, 2015

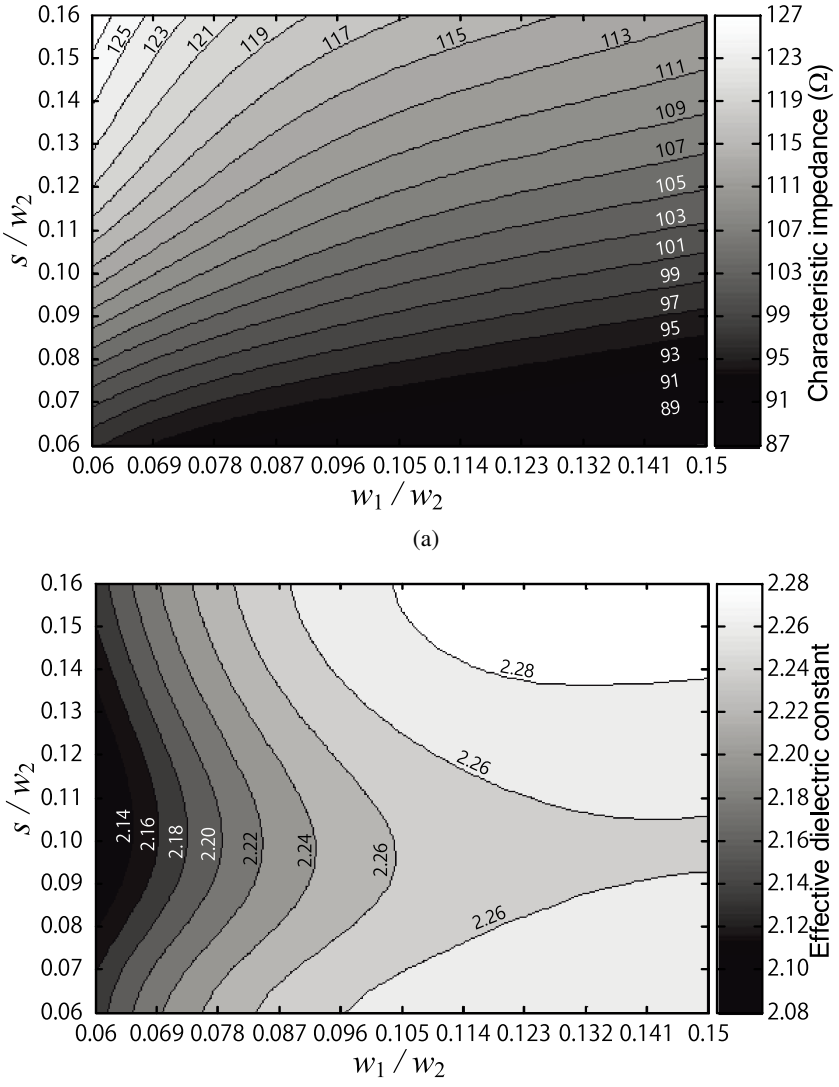

Fig. 6. Effective dielectric constant and characteristic impedance of asymmetric CPS on a single layer dielectric with $h_{b1} = 0.5w_1$ and $\varepsilon_{b1} = 4.6$: (a) characteristic impedance and (b) effective dielectric constant.

4 Conclusion

The mode-matching method was applied to the analysis of symmetric and asymmetric CPS surrounded by multilayer dielectrics. The characteristic impedances and the effective dielectric constants for various CPS on multilayer dielectrics were estimated. Based on the validation of the quasi-static analysis, the accuracy of the mode-matching method was verified in comparison with the conformal mapping technique. The presented formulation and the analyses for various CPS structures would provide useful information for the design of diverse microwave components using CPSs.

Acknowledgments

This work was supported by the Korea Research Institute of Standards and Science under the project 'Development of Technologies for Next-generation Electromagnetic Wave Measurement Standard,' grant 15011014.

© IEICE 2015
DOI: 10.1587/elex.12.20150361
Received April 17, 2015
Accepted May 11, 2015
Publicized June 11, 2015
Copyedited September 10, 2015